Published in final edited form as:
Exp Neurol. 2014 June ; 256: 25–38. doi:10.1016/j.expneurol.2014.03.016.

CD36 deletion improves recovery from spinal cord injury

Scott A. Myers[a,b], **Kariena R. Andres**[a,b], **Theo Hagg**[a,b,d,1], and **Scott R. Whittemore**[a,b,c,*]

[a]Kentucky Spinal Cord Injury Research Center, University of Louisville School of Medicine, 511 S. Floyd St., Rm. 616A, Louisville, KY 40202, USA

[b]Department of Neurological Surgery, University of Louisville School of Medicine, 511 S. Floyd St., Rm. 616A, Louisville, KY 40202, USA

[c]Department of Anatomical Sciences and Neurobiology, University of Louisville School of Medicine, 500 S. Preston St., Rm 916A, Louisville, KY 40202, USA

[d]Department of Pharmacology and Toxicology, University of Louisville School of Medicine, 500 S. Preston St., Louisville, KY 40202, USA

Abstract

CD36 is a pleiotropic receptor involved in several pathophysiological conditions, including cerebral ischemia, neurovascular dysfunction and atherosclerosis, and recent reports implicate its involvement in the endoplasmic reticulum stress response (ERSR). We hypothesized that CD36 signaling contributes to the inflammation and microvascular dysfunction following spinal cord injury. Following contusive injury, $CD36^{-/-}$ mice demonstrated improved hindlimb functional recovery and greater white matter sparing than $CD36^{+/+}$ mice. $CD36^{-/-}$ mice exhibited a reduced macrophage, but not neutrophil, infiltration into the injury epicenter. Fewer infiltrating macrophages were either apoptotic or positive for the ERSR marker, phospho-ATF4. $CD36^{-/-}$ mice also exhibited significant improvements in injury heterodomain vascularity and function. These microvessels accumulated less of the oxidized lipid product 4-hydroxy-trans-2-nonenal (4HNE) and exhibited a reduced ERSR, as detected by vascular phospho-ATF4, CHOP and CHAC-1 expression. In cultured primary endothelial cells, deletion of CD36 diminished 4HNE-induced phospho-ATF4 and CHOP expression. A reduction in phospho-eIF2α and subsequent increase in KDEL-positive, ER-localized proteins suggest that 4HNE-CD36 signaling facilitates the detection of misfolded proteins upstream of eIF2α phosphorylation, ultimately leading to CHOP-induced apoptosis. We conclude that CD36 deletion modestly, but significantly, improves functional recovery from spinal cord injury by enhancing vascular function and reducing macrophage infiltration. These phenotypes may, in part, stem from reduced ER stress-induced cell death within endothelial and macrophage cells following injury.

*Corresponding author at: Kentucky Spinal Cord Injury Research Center, Department of Neurological Surgery, University of Louisville School of Medicine, MDR616, 511 South Floyd Street, Louisville, KY 40202, USA. Fax: +1 502 852 5148. haggt1@etsu.edu (T. Hagg), swhittemore@louisville.edu (S.R. Whittemore). .
[1]Current address: Department of Biomedical Sciences, East Tennessee State University, Johnson City, TN 37614, USA.

Supplementary data to this article can be found online at http://dx.doi.org/10.1016/j.expneurol.2014.03.016.

Keywords

CD36; Spinal cord injury; Endoplasmic reticulum stress response; Microvasculature; Inflammation; Macrophage

Introduction

Contusion of the spinal cord leads to secondary complications including loss of spinal microvasculature, induction of inflammatory responses and oxidative damage. These responses exacerbate cell death, axonal degeneration, and demyelination within the contusion and injury penumbra (Alexander and Popovich, 2009; Mautes et al., 2000). Early vessel dysfunction and subsequent edema contribute to the infiltration of inflammatory cells (Mautes et al., 2000; Popovich and Longbrake, 2008). Blocking neutrophil and macrophage influx into the contusion leads to neuroprotection and improved locomotor function (Gris et al., 2004; Popovich and Jones, 2003). An initial loss of epicenter vasculature is followed by an angiogenic response 3 to 7 days following spinal cord injury (SCI), but these new vessels are immature and leaky (Benton et al., 2008; Casella et al., 2002; Loy et al., 2002; Whetstone et al., 2003). This later phase of microvascular instability has been hypothesized to contribute to chronic histopathology following SCI (Casella et al., 2002; Loy et al., 2002). Stabilization of epicenter and penumbral vasculature facilitates tissue sparing and functional recovery following SCI (Han et al., 2010).

Following SCI, cells with high protein secretory capacity initiate the unfolded protein response (UPR) to minimize toxic aggregation of misfolded proteins in the endoplasmic reticulum (ER) (Aufenberg et al., 2005; Ohri et al., 2011; Sakurai et al., 2005). Endothelial cells also initiate the UPR after ER sensors detect a high unfolded/misfolded protein to ER chaperone ratio (Marciniak et al., 2006; Yoshida, 2007). ER stress within endothelial cells contributes to many diseases, including hypertension, atherosclerosis, diabetes and bleeding disorders (Witte and Horke, 2011). Activation of the UPR leads to phosphorylation of the translation initiation protein eIF2α, which inhibits global translation in order to reduce ER-localized, KDEL-tagged proteins and minimize exacerbation of ER stress. eIF2α-independent genes such as activating transcription factor 4 (ATF4), which regulates the expression of other transcription factors, are upregulated to overcome this stress (Witte and Horke, 2011). Endothelial cells that cannot restore homeostasis induce expression of the pro-apoptotic proteins C/EBP (CCAAT enhancer binding protein) homologous protein (CHOP) and cation transport regulator-like protein 1 (CHAC-1) downstream of ATF4 (Mungrue et al., 2009). $CHOP^{-/-}$ mice exhibit a reduced inflammatory response, improved vascular sparing and enhanced locomotor recovery following SCI (Fassbender et al., 2012; Ohri et al., 2011). This improved vascular sparing coincides with a peak of lipid peroxidation, oxidative damage and accumulated protein adducts of 4HNE (Carrico et al., 2009), the most abundant unsaturated aldehyde generated in oxidized lipids by reactive oxygen species (Benedetti et al., 1980). Oxidized phospholipids, including 4HNE, induce ER stress in endothelial cells (Mungrue et al., 2009; Vladykovskaya et al., 2012), and these ligands trigger ERSR-induced apoptosis in macrophages through a CD36-dependent mechanism (Seimon et al., 2010).

CD36, an 88 kDa glycoprotein, is a multifunctional receptor that contributes to several pathophysiological conditions, including cerebral ischemia (Cho et al., 2005; Kunz et al., 2008), neurovascular dysfunction (Park et al., 2011) and atherosclerosis (Febbraio et al., 2000; Harb et al., 2009). High affinity CD36 agonists include lipid peroxidation products such as 4HNE (Silverstein et al., 2010) and thrombospondin-1 (TSP-1). CD36 is expressed in a variety of tissues, including macrophages and endothelial cells, and regulates inflammation (Oh et al., 2012; Seimon et al., 2010) and angiogenesis (Jimenez et al., 2000). Due to its pharmacologic accessibility and multiple pathogenic downstream pathways, CD36 has been proposed to be an ideal molecular target for developing clinically relevant therapeutic strategies for neurodegenerative diseases (Cho and Kim, 2009).

The goal of this study was to assess the role of CD36 signaling on the secondary pathophysiological effects following SCI. We hypothesized that CD36 signaling contributes to the inflammation and microvascular dysfunction following injury. These effects were assessed in a contusive SCI model in $CD36^{-/-}$ mice.

Materials and methods

Reagents

FITC-LEA (*Lycopersicon esculentum* agglutinin lectin; FL-1171) was purchased from Vector Labs (Burlingame, CA). TRITC (1:200)-, FITC (1:200)-, CY5 (1:200) or AMCA (1:100)-conjugated donkey secondary antibody $F(ab')_2$ fragments and normal donkey serum (017-000-121) were purchased from Jackson Immunoresearch (West Grove, PA). TRITC (1:200)-conjugated goat anti-mouse IgA (MBS674424) was purchased from MyBioSource.com. Mouse collagen IV (#354233) was purchased from BD Biosciences (San Jose, CA). Plasma-derived serum (BT-214) was purchased from Biomedical Technologies Inc. (Stoughton, MA). Collagenase type 1 (4196) was purchased from Worthington Biologicals (Lakewood, NJ). Endothelial cell growth supplement (#02102) was purchased from Millipore (Billerica, MA). Twenty μm (CMN-0020-D) and 500 μm (CMN-0500-D) mesh filters were purchased from smallparts.com. Heparin (H4784), percoll (P1644), puromycin (P8833), DNase I (DN25), XTT (TOX2), guanabenz (G110) and dextran (D4876) were purchased from Sigma (St. Louis, MO). 4HNE (4-hydroxynonenal, #75899-68-2) was purchased from Cayman Chemical (Ann Arbor, MI). Boehringer Protease inhibitor cocktail (#11330800) was purchased from Roche (Mannheim, Germany). BCA Protein Assay Kit (#23225) was purchased from Thermo Scientific (Waltham, MA). Nitrocellulose membranes were purchased from Whatman (Schleicher & Schuell, London, U.K.). Salubrinal (ALX-270-428) was purchased from Enzo Life Sciences (Farmingdale, NY).

Surgical procedures

All surgical intervention, care, and treatment of animals were in strict accordance with the PHS Policy on Humane Care and Use of Laboratory Animals (National Research Council, 1996) and University of Louisville IACUC and Institutional Biosafety Committee guidelines. The genetic backgrounds of all strains used in this study were C57BL/6. WT mice were obtained from Harlan (Indianapolis, IN). $CD36^{-/-}$ mice were a kind gift from

Costantino Iadecola (Weill Cornell Medical College, NY). Adult (6–8 weeks old, 18–22 g) female C57BL/6 mice were used in this study and anesthetized using a 2.0% avertin solution (2,2,2-tribromoethanol) administered at 240 mg/kg IP and prepared as described (Benton et al., 2008). Mice received sham T10 laminectomies or 50 kdyn contusions using the IH impactor (Infinite Horizons Inc., Lexington, KY) as described (Benton et al., 2008; Mahoney et al., 2009; Scheff et al., 2003). For functional assessment, mice were scored by the Basso Mouse Scale (BMS) (Basso et al., 2006) one week prior to surgery and weekly after SCI. All raters were trained and certified at OSU by Dr. Basso and were blinded to genotype/treatment group.

Treadscan analysis

Recording and analysis of mice placed on a motor-driven translucent treadmill were performed as described (Beare et al., 2009), except the blinded scorer set the treadmill at the best walking speed for each untrained mouse, as determined by slowly increasing the treadmill speed until the animal was consistently walking with minimal lateral/longitudinal movement (Beare et al., 2011). Locomotion was recorded from below at 100 frames/s, and TreadScan software (CleverSys, Reston, VA) was used to track and quantify overall run speed mean instantaneous and overall run speed, hindlimb swing time, stride length, toe spread, and rear track width. Baseline TreadScan analysis was performed 3 days prior to injury. Post-injury TreadScan analysis was performed at 7 weeks post-SCI.

Tissue processing, immunohistochemistry, and immunocytochemistry

At the end of the experiment, mice were anesthetized IP with a 2.0% avertin solution (10 mg) and 100 μg of FITC-LEA in 100 μl PBS was delivered systemically via the surgically exposed right external jugular vein and allowed to circulate for 15 min prior to transcardial perfusion with 20 ml PBS, pH 7.4. LEA is a lectin that exhibits spec-ificity for N-acetyl-D-glucosamine-β(1,4)N-acetyl-D-glucosamine oligomers, and when delivered intravascularly, has been widely used to identify perfused microvessels in various tissues (Benton et al., 2008; Jilani et al., 2003; Thurston et al., 1996). Quantitation of LEA staining 1.5 mm rostral and caudal to the contusion (outside the injury penumbra) demonstrated no significant difference in the perfusion of the spinal microvasculature by the intravital dye between groups (data not shown). Spinal cords were dissected, snap frozen, and longitudinally sectioned at 20 μm on a cryostat. Sections were thaw mounted on microscope slides (Fisher Scientific, Pittsburgh, PA) and stored at −80 °C. Slides were warmed at 37 °C for 10 min and fixed in ice-cold methanol for 20 min. Isolated endothelial cells or microvessels (see below) were washed 3× with PBS and either fixed in 4% PFA for 1 h at 25 °C, or with methanol for 20 min at −20 °C for the detection of PFA-sensitive antigens. Cords or cells were blocked in TBS + 0.1% Triton X-100, 0.5% BSA, and 10% normal donkey serum for 1 h at 25 °C and then incubated overnight at 4 °C with primary antibodies (Table 1) in a blocking buffer, followed by incubation in secondary antibodies at 25 °C for 1 h. Negative controls included appropriate species-specific non-immune Ig subtypes instead of primary antibodies.

For assessment of white matter sparing, animals were anesthetized IP with avertin and spinal cords were dissected after transcardial perfusion with PBS and 4% PFA. Cords were

submerged in 4% PFA overnight at 4 °C, stored in a 30% sucrose solution for 72 h at 4 °C, and cut serially in 20 μm coronal sections on a cryostat 1 cm caudal and rostral to the injury epicenter. Sections were thaw mounted on microscope slides and stored at −80 °C. Eriochrome cyanine staining was performed to delineate spared myelin (Magnuson et al., 2005; Scheff et al., 2003).

Image quantitation

Confocal imaging was performed on an Olympus FV1000 confocal microscope equipped with 488 (for visualizing FITC), 543 (TRITC), and 633 (CY5) laser lines. Confocal stacks were obtained (0.5 μm step size) using a 40 × objective. Images were then opened in Nikon Elements software (Nikon Instruments, Melville, NY) and rendered for volume and co-localization of fluorophores. All other images were captured with a Nikon TE 300 inverted microscope equipped with a Spot CCD camera using identical exposure settings. For all tissue assessments, every fifth horizontal/longitudinal section (11–12 20 μm sections) from each cord was stained and photographed with a 10× objective and stitched with Elements software during acquisition. Elements software was used to threshold baseline brightness and contrast identically for each image for all quantitative object and field measurements. The areas of the regions of interest were centered on the contusion epicenters and quantified by a scorer blinded to genotype or treatment. The injury epicenter was defined as the domain exhibiting significant extravascular deposition and disorganization of vascular laminin [3, 7 days post-injury (dpi)] or GFAP immunoreactivity [1, 3, 7 dpi] (Benton et al., 2008; Whetstone et al., 2003). The injury penumbra was defined as 500 μm rostral and caudal to the epicenter (Fassbender et al., 2011; Myers et al., 2011). The injury core, or heterodomain, was defined as the area including both the epicenter and penumbra. The mean areas quantified from the injured cords were used to define the regions of interest used to quantify sham control cords at roughly T10 (Benton et al., 2008).

To assess the presence of inflammatory markers, the total area within the injury heterodomain positive for either Iba1, CD16/32, CD45 or CD68 was quantified by digital image analysis using the basic densitometric thresholding features of Elements software, similar to methods previously reported (Donnelly et al., 2009). Threshold values were obtained and set for each marker and held constant for each image quantified. For quantitation of ER stressed inflammatory cells, the total number of cleaved caspase-3 or phospho-ATF4 positive cells that co-localized with either CD45 or CD16/32, respectively, within the injury epicenter were counted. For assessment of contusion vascularity, the percentage of the heterodomain area positive for platelet endothelial adhesion molecule (CD31) microvessels was quantified. For assessment of microvessel patency, the percentage area of heterodomain CD31-positive microvessels that co-localized with LEA staining was quantified. For assessment of ER stressed microvasculature, the percentage area of heterodomain CD31-positive microvessels co-localized with either 4HNE, CHOP or CHAC-1 was quantified, excluding phospho-ATF4, in which individual $CD31^+$ microvessel nuclei within the heterodomain were counted. For assessment of neutrophil infiltration, Elements software thresholding was performed using identical parameters within the ‘Object Count’ feature to define neutrophil counting criteria based on size, circularity, and intensity. For assessment of in vitro endothelial cell proliferation, the percentage of total nuclei

expressing the proliferative marker Ki67 was quantified within 4 fields in each of 3 separate 96-wells, each within 3 independent experiments.

For white matter sparing, every other section throughout roughly 1.5 mm of the injured spinal cords was captured. Images were coded and randomized to facilitate unbiased, blinded quantification using densitometric thresholding features of Elements (Nikon) software. The epicenter of each injury was defined as the section with the lowest amount of white matter. The data were then normalized to spared white matter in corresponding sham sections.

Statistical analyses

For functional assessments after injury, a mixed model repeated measures ANOVA and Bonferroni post hoc t-tests were used to compare differences between groups for BMS means. For BMS subscores, Mann–Whitney non-parametric t-tests were performed. For analyzing spared white matter, mean values of percent spared white matter area were compared using a mixed model repeated measures ANOVA with Bonferroni post hoc t-tests. For all other analyses, two-tailed Student's t-tests assuming equal variance were performed.

Cell culture

Primary murine cortex endothelial cell isolation was adapted from protocols as described (Hoying et al., 1996). Briefly, cortices from 6 to 8 week old mice were removed and aseptically dissected in L15 media/2% FBS. Cortices were minced and incubated for 45 min at 37 °C in 2 mg/ml collagenase/1 mg/ml DNase I. Homogenates were washed in PBS, resuspended in 15% dextran, and spun at 4000 ×*g* for 20 min. The microvascular pellet was resuspended in PBS, passed through a 500 μm screen, and collected on a 20 μm screen. Microvessels were washed in PBS, pelleted, and resuspended in DMEM/F12 with 20% platelet-derived serum (PDS), 100 μg/ml endothelial cell growth supplement, 80 μg/ml heparin, and 4 μg/ml puromycin. Microvessels were plated into 35 mm^2 dishes precoated with 5 $\mu g/cm^2$ murine collagen IV at a density of 150,000 microvessels/cm^2. The puromycin was removed after 2–3 days, leaving 95–99% pure endothelial cell cultures as assessed by CD31 and α-actin (smooth muscle cell) immunocytochemistry. After reaching confluency, 96-well dishes were seeded at 50,000 cells/cm^2. Cells were incubated in DMEM/F12 + 1% PDS with 17.5 μM 4HNE or vehicle control for 6 h at 37 °C/5% CO_2 for assessment of ERSR markers. For XTT cell proliferation assays, cells were incubated in DMEM/F12 + 20% PDS with antibodies for 18 h prior to addition of XTT. Plates were allowed to develop for 6 h and read at 450 nm and 690 nm on an ELISA plate reader, according to the manufacturer's instructions. All experiments were performed using passage 1–2 endothelial cells.

For Western analyses, 35 mm^2 dishes of confluent passage 1 cortical endothelial cells were pretreated with either vehicle, 100 μM salubrinal, or 100 μM guanabenz for 30 min. prior to a 6 h treatment of vehicle or 17.5 μM 4HNE in DMEM/F12 + 1% PDS at 37 °C/5% CO_2. Cells were washed twice with PBS, resuspended in lysis solution (10 mM Tris–HCl, pH 7.4, 1% SDS, 4 mg/ml Boehringer protease inhibitor cocktail) and sonicated briefly. Protein concentrations were determined by BCA assay. Thirty μg of protein was separated by 10%

SDS-PAGE, transferred to nitrocellulose membranes, blocked in TBS-T, 5% milk and immunostained.

Results

Deletion of CD36 improves functional recovery following SCI

Assessment of locomotor function after moderate contusion of the T10 spinal cord revealed that CD36$^{-/-}$ mice exhibited a statistically significant improvement in recovery relative to WT, beginning three weeks following injury (Fig. 1A). This improvement was sustained up to six weeks after injury (the final time point examined). The increase in motor function above a score of 5 is significant in this non-linear scale as it reflects the restoration of the capacity for plantar stepping and weight support. BMS subscore analysis revealed a significantly greater number of CD36$^{-/-}$ mice with improved motor function beginning two weeks post-injury, with primarily an improvement in hindlimb coordination relative to WT mice (Fig. 1B). Despite receiving injuries of comparable severity, as assessed by impact displacement (Fig. 1C) and force (Fig. 1D), the contusion lesion epicenters of CD36$^{-/-}$ mice were significantly smaller, as assessed by laminin deposition (Fig. 1E) and GFAP expression (Fig. 1F). No significant differences in morbidity or mortality (91% versus 96% survival rate for WT and CD36$^{-/-}$, respectively) were observed.

At 7 weeks post-injury, TreadScan analysis (Beare et al., 2009; Beare et al., 2011) revealed a small but significant increase in the mean rear toe spread in CD36$^{-/-}$ mice relative to WT following injury (Supplemental Fig. 1B), but not prior to injury (Supplemental Fig. 1B). A narrowing of hindlimb toe spread follows sciatic nerve crush in mice (Blakeman et al., 2003; Hygge-Blakeman et al., 2004), and hindlimb toe spread has been correlated with SCI severity (Beare et al., 2009), with injuries of increasing severity, as assessed by the BMS, leading to narrower toe spread. The significantly wider toe spread in CD36$^{-/-}$ mice may stem from improved balance, truck stability and/or hindlimb sensory motor function following injury. No significant differences, however, were observed between groups in hindlimb swing time, stride length, rear track width, or either instantaneous or overall run speed, either before (data not shown) or following injury (Supplemental Fig. 1). These data together suggest that CD36 ablation modestly improves recovery from contusive spinal cord injury.

Deletion of CD36 improves spared white matter after SCI

A correlation between the degree of epicenter white matter sparing following contusive injury and the extent of functional recovery as assessed by BMS has been established (Basso et al., 2006). To determine whether CD36 expression had a chronic effect on lesion size following moderate contusion, the degree of spared white matter throughout the contused cords seven weeks following injury was assessed (Fig. 1G). Eriochrome cyanine staining revealed that CD36$^{-/-}$ mice exhibited significantly more spared white matter at the injury epicenter (32.6% ± 3.0) relative to WT mice (20.4% ± 4.3), and these percentages correlate well with predicted BMS values (Basso et al., 2006) and their actual BMS values at 6 weeks post-injury. This increase in sparing was especially prominent caudal to the injury epicenter

(Fig. 1G). These data indicate that the increased white matter at the contusion epicenter contributes to the enhanced behavioral recovery from injury in CD36$^{-/-}$ mice.

Ablation of CD36 reduces macrophage responses following SCI

Following moderate spinal cord contusion in mice, CD36 mRNA becomes detectable in whole epicenter homogenates by 1 dpi, peaks at 7 dpi, and returns almost to baseline by 28 dpi (Edgar et al., 2002). Consistent with its mRNA expression profile, CD36 protein is not detectable in either sham uninjured spinal cords (Fig. 2A), or 1 mm rostral or caudal to the contusion epicenter (data not shown). Immunohistochemical analysis revealed that early expression of CD36 is primarily localized within the spinal microvasculature, particularly within under-perfused microvessels, as determined by the absence of co-localization with the perfusion marker, LEA (Figs. 2B, C). By 7 dpi, CD36 is no longer detectable within CD31-expressing microvessels, but is strongly expressed in invading CD45-positive inflammatory cells (Figs. 2D–E). No CD36 protein is detectable in CD36$^{-/-}$ mice (Fig. 2F).

Consistent with its known expression on macrophages, CD36$^{-/-}$ mice exhibited a reduction in heterodomain-localized inflammatory cells following injury. The area of heterodomain-localized inflammatory cells expressing the markers Iba1 (Figs. 3A, B, E), CD16/32 (Figs. 3C, D, F), CD45 (Figs. 4A, B, E) and CD68 (Figs. 4C, D, F) were all significantly reduced in CD36$^{-/-}$ mice by 7 dpi, with only Iba1 not exhibiting a significantly different response at 3 dpi. Of the CD45- or CD16/CD32-expressing inflammatory cells localized within the contusion epicenter at 7 dpi, ablation of CD36 reduced the number of cells expressing either cleaved caspase-3 (CC3; Figs. 5A, B, E), a marker for apoptosis, or phosphorylated activating transcription factor 4 (pATF4; Figs. 5C, D, F), a marker for ER stress, respectively. Confocal imaging con-firmed the localization of cleaved caspase-3 or phospho-ATF4 within epicenter-localized CD45 or CD16/32-positive inflammatory cells, respectively (Figs. 5G, H). Ablation of CD36 appeared to have no effect on neutrophil migration and invasion into the contusion heterodomain at either 1 or 3 dpi, as assessed by quantification of 7/4-positive polymorphonuclear cells (Supplemental Figs. 2A–C).

Deletion of CD36 rescues heterodomain microvasculature following SCI

As CD36 expression localizes primarily within the microvasculature of the lesion epicenter (Figs. 2B, C) immediately following injury, and given the known anti-angiogenic effects of CD36 (Dawson et al., 1997), we quantified the CD31-expressing microvasculature following contusion (Figs. 6A, B). Ablation of CD36 modestly increased vascularity within the injury heterodomain as early as 1 dpi (Fig. 6C). At 3 dpi, a time point in the mouse during which epicenter vascularity begins to increase following initial trauma (Benton et al., 2008; Whetstone et al., 2003), ablation of CD36 appeared to have even more significant effects on microvessel sparing and/or angiogenesis (Fig. 6C). Consistently, genetic ablation or antibody functional blockade of CD36 led to significant increases in CNS-derived endothelial cell proliferation in vitro, as assessed by the proliferation marker Ki67 (Figs. 6E–G), or metabolism of the cell viability substrate XTT (Fig. 6H), respectively. In addition to its effects on microvascular angiogenesis/ sparing in vivo, deletion of CD36 also leads to improvements in vascular function following injury. As assessed by intravital staining of the vascular lumen with the perfusion marker LEA, a small but significant improvement in the

perfusion status of the injury heterodomain vasculature was observed in CD36$^{-/-}$ mice at 3 dpi (Fig. 6D), although no significant difference was observed at 1 dpi. By 7 weeks post-injury, however, the extent of spared epicenter vascularity as assessed by PECAM immunoreactivity in CD36$^{-/-}$ mice was not significantly different from WT animals (data not shown).

CD36 ablation decreases vascular oxidative stress and ER stress responses after SCI

To investigate the effects of CD36 on acute vascular sparing following contusion, we quantified the localization of 4HNE, a marker for oxidative stress, within the vascular compartment of the injury heterodomain (Figs. 7A, B, H). While endogenous levels of 4HNE are produced in the absence of injury, these levels increase significantly by 1 dpi. By 3 dpi, 4HNE levels within the heterodomain vasculature are significantly lower in CD36$^{-/-}$ mice relative to WT (Fig. 7H). Confocal imaging revealed co-localization of 4HNE within the CD31^{+} microvasculature (Fig. 7J). We also quantified the localization of some markers of the ER stress response within the vascular compartment of the spinal cord following injury. The heterodomain microvasculature of CD36$^{-/-}$ mice contained significantly fewer nuclei positive for phospho-ATF4 than WT at both 1 and 3 dpi (Figs. 7F, G, I, K). Similarly, significantly fewer microvessels within the injury heterodomain of CD36$^{-/-}$ mice co-localized with CHOP at both 1 and 3 dpi (Figs. 8A, B, E, G). Contusive injury induced the expression of the pro-apoptotic cation transport regulator-like protein 1 (CHAC-1) within the microvasculature by 1 dpi, and a significantly lower expression within CD36$^{-/-}$ microvessels was apparent by 3 dpi (Figs. 8C, D, F, H). Therefore, not only are there more surviving and/or angiogenic microvessels within the acutely injured heterodomain of CD36$^{-/-}$ mice, but of those existing microvessels, a lower percentage of them are expressing markers of ER stress relative to WT.

Exogenous 4HNE induces diminished ERSR in CD36$^{-/-}$ endothelial cells in vitro

To determine the effects of CD36 on the expression of downstream ER stress response proteins, 4HNE was applied to isolated, CNS-derived endothelial cells. After a 6 h incubation with 17.5 μM 4HNE, a significantly lower percentage of CD36$^{-/-}$ endothelial cells expressed either CHOP (Figs. 9A, B, G) or phospho-ATF4 (Figs. 9C, D, H) relative to WT endothelial cells. Although all endothelial cells retained KDEL-positive, ER-localized proteins even in the absence of 4HNE, CD36$^{-/-}$ endothelial cells expressed significantly more than WT endothelial cells, as determined by the percentage area of the CD31-positive cell body (Figs. 9E, F, I). Consistent with a defect in the ER stress response, phosphorylation of eIF2α, which inhibits global translation, was significantly reduced in CD36$^{-/-}$ endothelial cells (Fig. 9J). Even in the presence of the phosphatase inhibitors salubrinal or guanabenz, which increase phosphorylation of eIF2α, levels of phospho-eIF2α remained low in CD36$^{-/-}$ endothelial cell lysates (Figs. 9J, K).

Discussion

While uninjured CD36$^{-/-}$ mice appear phenotypically normal overall (Febbraio et al., 1999), these mice exhibit reduced dysfunction and disease progression to a variety of injuries including ER stress, stroke, Aβ toxicity, and oxLDL-atherosclerosis (Cho et al., 2005; Oh et

al., 2012; Park et al., 2009; Rahaman et al., 2006). CD36 can reduce injury progression after stroke in neonate mice via its role in monocyte/macrophage infiltration and phagocytosis of apoptotic bodies (Woo et al., 2012). However, the reactive oxygen species production, oxidative stress, glial scar formation and post-ischemic inflammation prominent in many adult injury models are at least partially regulated by CD36 and are diminished by its absence (Bao et al., 2012; Cho and Kim, 2009; Kunz et al., 2008; Park et al., 2011).

Consistent with these adult injury models, our results reveal that deletion of CD36 leads to a reduction in lesion volume, heterodomain macrophage localization and vascular ERSR, resulting in an improvement in functional recovery following SCI. Knockout of CD36 leads to improvements in vascularity within the injury heterodomain at both 1 and 3 days post-injury, but not by 7 weeks post-injury. The angiogenic response that follows SCI in wildtype mice does not begin until 3 dpi (Benton et al., 2008). Therefore, the early vascular improvements observed at 1 dpi in $CD36^{-/-}$ mice may be due to increased vascular sparing. CD36 activation induces apoptosis in endothelial cells (Jimenez et al., 2000), and we observed a decrease in vascular CHOP expression following injury in $CD36^{-/-}$ mice. $CHOP^{-/-}$ mice exhibit improved vascular sparing and functional recovery following SCI (Fassbender et al., 2012; Ohri et al., 2011). Alternatively, $CD36^{-/-}$ mice may exhibit an earlier angiogenic response following injury. Consistently, our results show that abrogation of CD36 signaling in CNS-derived endothelial cells increases proliferation in vitro. An improved angiogenic response is consistent with the known anti-angiogenic function of CD36 (Jimenez et al., 2000).

Abrogation of CD36 signaling also leads to an increase in vascular perfusion within the injury heterodomain at 3 dpi. CD36 is known to negatively regulate endothelial nitric oxide synthase and cGMP production in endothelial cells, leading to vasoconstriction (Isenberg et al., 2008), and the increased CD36 mRNA (Edgar et al., 2002) and protein localization to hypoperfused microvessels within the epicenter are consistent with a role for CD36 in regulating vascular hemodynamics following SCI. The increased vascularity and improved perfusion status may both contribute to the reduced lesion volume and overall acute functional improvements following injury.

Products of oxidative damage such as the abundant polyunsaturated aldehyde 4HNE accumulate within the spinal cord contusion epicenter as early as 3 h post-injury, peaking at 3 dpi (Carrico et al., 2009). 4HNE also has been shown to induce the ERSR in endothelial cells (Vladykovskaya et al., 2012). The spinal microvasculature of $CD36^{-/-}$ mice exhibits a reduced ERSR following injury. While the ERSR proteins phospho-ATF4 and CHOP were significantly down-regulated in $CD36^{-/-}$ microvessels as early as 1 dpi, 4HNE accumulation was not significantly different from WT microvessels until 3 dpi. Several bioactive oxidized phospholipids, in addition to 4HNE, interact with and induce their pathogenic effects via an interaction with CD36 at truncated fatty acids at the sn-2 position (Berliner et al., 2009). It is highly likely that 4HNE is not the only lipid peroxidation product that induces ER stress in microvessels following SCI. The pro-apoptotic protein CHAC-1 is upregulated in endothelial cells following exposure to oxidized phospholipids or ERSR inducers (Gargalovic et al., 2006b; Mungrue et al., 2009). While CHAC-1 is upregulated within the vasculature by 1 dpi, significant differences in expression are not seen within $CD36^{-/-}$ mice

until 3 dpi. This delayed expression profile may reflect its activation downstream of ATF4 and CHOP signaling.

The mechanism by which CD36 regulates ER stress signaling is currently unknown. 4HNE-induced apoptosis is dependent upon de novo protein synthesis (West and Marnett, 2005). $CD36^{-/-}$ endothelial cells exhibit a reduced ability to induce phosphorylation of eIF2α. This inability would presumably lead to a reduced ability to inhibit global translation following ER stress and a subsequent increase in unfolded/misfolded, KDEL-positive proteins within the ER. These results suggest that CD36 is part of the signaling machinery necessary to detect protein accumulation within the ER and initiate the ERSR. Following induction of ER stress, the unfolded protein response can directly promote NF-κB activation through a PERK-eIF2α-mediated attenuation of translation (Deng et al., 2004; Wu et al., 2004). Consistently, activation of NF-κB is attenuated in $CD36^{-/-}$ mice following cerebral ischemia (Kunz et al., 2008), though the signaling mechanisms by which this occurs is not fully understood.

$CD36^{-/-}$ mice exhibit a reduction in the presence of heterodomain-localized macrophages following SCI. While our data cannot determine the mechanism for this difference, several possibilities exist. Pharmacologic inhibition of CD36 reduces levels of CCL2, circulating IL-6 and subsequent mononuclear phagocyte trafficking to sites of atherosclerotic lesions (Harb et al., 2009). $CD36^{-/-}$ macrophages also exhibit reduced CCL2-stimulated chemotaxis (Kuchibhotla et al., 2008). The decrease in heterodomain macrophages in $CD36^{-/-}$ mice may therefore result from a combination of reduced chemokine release and defective macrophage chemotactic responses following SCI. $CHOP^{-/-}$ mice exhibit improved vascularity and reduced macrophage infiltration following injury (Fassbender et al., 2012). Lower ERSR-induced apoptosis in these mice may lead to less inflammation and reduced production of macrophage-recruiting chemokines. The reduced localization of the lipid peroxidation product 4HNE and CHOP expression within the vasculature of $CD36^{-/-}$ mice would be consistent with a reduced recruitment of macrophages to the injury epicenter. Other oxidized phospholipids and agonists of CD36 regulate monocyte trafficking through the upregulation of CCL2, IL8, IL6, MCP1 and CXCL3 within the endothelial lining in an ERSR-dependent fashion (Boring et al., 1998; Dawson et al., 1999; Gargalovic et al., 2006a). Once present at the injury site, $CD36^{-/-}$ macrophages may produce fewer reactive oxygen species and induce less oxidative damage (Zhou et al., 2011). CD36 also mediates oxidized phospholipid-initiated, ER stress-induced apoptosis in macrophages (Seimon et al., 2010). Therefore, a further potential source of reduced inflammation and monocyte recruitment in $CD36^{-/-}$ mice may be the reduced apoptosis of recruited, epicenter localized macrophages. Indeed, within the injury epicenter, recruited macrophages expressed less phospho-ATF4 and cleaved-caspase 3 in $CD36^{-/-}$ mice after SCI.

In conclusion, knockout of CD36 signaling leads to a reduced lesion volume, decreased inflammation, improved acute heterodomain vascularity and microvascular perfusion, and a reduced vascular ERSR. These effects in combination likely lead to the functional improvements observed following SCI.

Supplementary Material

Refer to Web version on PubMed Central for supplementary material.

Acknowledgments

This work was supported by NS045734 (NIH R01 NS045734), RR1556/GM103507 (NIHP30 RR1556/GM103507), the Kentucky Spinal Cord and Head Injury Research Trust, Norton Healthcare, and the Commonwealth of Kentucky Research Challenge for Excellence Trust Fund (S.R.W., T.H.). We thank Christine Yarberry for surgical assistance, Jason Beare for confocal analysis, Kim Cash for animal care, Johnny Morehouse for BMS and Treadscan analyses, and Darlene Burke for statistical analyses.

Abbreviations

ERSR	endoplasmic reticulum stress response
4HNE	4-Hydroxy-trans-2-nonenal
ATF4	activating transcription factor 4
CHOP	(CCAAT enhancer binding protein) homologous protein
eIF2α	eukaryotic initiation factor 2α
SCI	spinal cord injury
UPR	unfolded protein response
TSP-1	thrombospondin-1

References

Alexander JK, Popovich PG. Neuroinflammation in spinal cord injury: therapeutic targets for neuroprotection and regeneration. Prog. Brain Res. 2009; 175:125–137. [PubMed: 19660652]

Aufenberg C, et al. Spinal cord trauma activates processing of xbp1 mRNA indicative of endoplasmic reticulum dysfunction. J. Neurotrauma. 2005; 22:1018–1024. [PubMed: 16156717]

Bao Y, et al. CD36 is involved in astrocyte activation and astroglial scar formation. J. Cereb. Blood Flow Metab. 2012; 32:1567–1577. [PubMed: 22510603]

Basso DM, et al. Basso Mouse Scale for locomotion detects differences in recovery after spinal cord injury in five common mouse strains. J. Neurotrauma. 2006; 23:635–659. [PubMed: 16689667]

Beare JE, et al. Gait analysis in normal and spinal contused mice using the TreadScan system. J. Neurotrauma. 2009; 26:2045–2056. [PubMed: 19886808]

Beare, JE., et al. Automated gait analysis following spinal cord injury. In: Chen, J., editor. Animal Models of Acute Neurological Injuries, II. Humana, Totowa, NJ: 2011.

Benedetti A, et al. Identification of 4-hydroxynonenal as a cytotoxic product originating from the peroxidation of liver microsomal lipids. Biochim. Biophys. Acta. 1980; 620:281–296. [PubMed: 6254573]

Benton RL, et al. *Griffonia simplicifolia* isolectin B4 identifies a specific subpopulation of angiogenic blood vessels following contusive spinal cord injury in the adult mouse. J. Comp. Neurol. 2008; 507:1031–1052. [PubMed: 18092342]

Berliner JA, et al. The role of oxidized phospholipids in atherosclerosis. J. Lipid Res. 2009; (Suppl. 50):S207–S212. [PubMed: 19059906]

Blakeman KH, et al. Hyperalgesia and increased neuropathic pain-like response in mice lacking galanin receptor 1 receptors. Neuroscience. 2003; 117:221–227. [PubMed: 12605908]

Boring L, et al. Decreased lesion formation in CCR2$^{-/-}$ mice reveals a role for chemokines in the initiation of atherosclerosis. Nature. 1998; 394:894–897. [PubMed: 9732872]

Carrico KM, et al. Temporal and spatial dynamics of peroxynitrite-induced oxidative damage after spinal cord contusion injury. J. Neurotrauma. 2009; 26:1369–1378. [PubMed: 19419247]

Casella GT, et al. New vascular tissue rapidly replaces neural parenchyma and vessels destroyed by a contusion injury to the rat spinal cord. Exp. Neurol. 2002; 173:63–76. [PubMed: 11771939]

Cho S, Kim E. CD36: a multi-modal target for acute stroke therapy. J. Neurochem. 2009; 109(Suppl. 1):126–132. [PubMed: 19393018]

Cho S, et al. The class B scavenger receptor CD36 mediates free radical production and tissue injury in cerebral ischemia. J. Neurosci. 2005; 25:2504–2512. [PubMed: 15758158]

Dawson DW, et al. CD36 mediates the In vitro inhibitory effects of thrombospondin-1 on endothelial cells. J. Cell Biol. 1997; 138:707–717. [PubMed: 9245797]

Dawson TC, et al. Absence of CC chemokine receptor-2 reduces atherosclerosis in apolipoprotein E-deficient mice. Atherosclerosis. 1999; 143:205–211. [PubMed: 10208497]

Deng J, et al. Translational repression mediates activation of nuclear factor kappa B by phosphorylated translation initiation factor 2. Mol. Cell. Biol. 2004; 24:10161–10168. [PubMed: 15542827]

Donnelly DJ, et al. An efficient and reproducible method for quantifying macrophages in different experimental models of central nervous system pathology. J. Neurosci. Methods. 2009; 181:36–44. [PubMed: 19393692]

Edgar R, et al. Gene Expression Omnibus: NCBI gene expression and hybridization array data repository. Nucleic Acids Res. 2002; 30:207–210. [PubMed: 11752295]

Fassbender JM, et al. Activating Notch signaling post-SCI modulates angiogenesis in penumbral vascular beds but does not improve hindlimb locomotor recovery. Exp. Neurol. 2011; 227:302–313. [PubMed: 21156172]

Fassbender JM, et al. Deletion of endoplasmic reticulum stress-induced CHOP protects microvasculature post-spinal cord injury. Curr. Neurovasc. Res. 2012; 9:274–281. [PubMed: 22873727]

Febbraio M, et al. A null mutation in murine CD36 reveals an important role in fatty acid and lipoprotein metabolism. J. Biol. Chem. 1999; 274:19055–19062. [PubMed: 10383407]

Febbraio M, et al. Targeted disruption of the class B scavenger receptor CD36 protects against atherosclerotic lesion development in mice. J. Clin. Invest. 2000; 105:1049–1056. [PubMed: 10772649]

Gargalovic PS, et al. The unfolded protein response is an important regulator of in-flammatory genes in endothelial cells. Arterioscler. Thromb. Vasc. Biol. 2006a; 26:2490–2496. [PubMed: 16931790]

Gargalovic PS, et al. Identification of inflammatory gene modules based on variations of human endothelial cell responses to oxidized lipids. Proc. Natl. Acad. Sci. U. S. A. 2006b; 103:12741–12746. [PubMed: 16912112]

Ghasemlou N, et al. Tissue displacement and impact force are important contributors to outcome after spinal cord contusion injury. Exp. Neurol. 2005; 196:9–17. [PubMed: 16023101]

Gris D, et al. Transient blockade of the CD11d/CD18 integrin reduces secondary damage after spinal cord injury, improving sensory, autonomic, and motor function. J. Neurosci. 2004; 24:4043–4051. [PubMed: 15102919]

Han S, et al. Rescuing vasculature with intravenous angiopoietin-1 and alpha v beta 3 integrin peptide is protective after spinal cord injury. Brain. 2010; 133:1026–1042. [PubMed: 20375135]

Harb D, et al. The role of the scavenger receptor CD36 in regulating mononuclear phagocyte trafficking to atherosclerotic lesions and vascular inflammation. Cardiovasc. Res. 2009; 83:42–51. [PubMed: 19264766]

Hoying JB, et al. Angiogenic potential of microvessel fragments established in three-dimensional collagen gels. In Vitro Cell. Dev. Biol. Anim. 1996; 32:409–419. [PubMed: 8856341]

Hygge-Blakeman K, et al. Galanin over-expression decreases the development of neuropathic pain-like behaviors in mice after partial sciatic nerve injury. Brain Res. 2004; 1025:152–158. [PubMed: 15464755]

Isenberg JS, et al. Thrombospondin-1: a physiological regulator of nitric oxide signaling. Cell. Mol. Life Sci. 2008; 65:728–742. [PubMed: 18193160]

Jilani SM, et al. Selective binding of lectins to embryonic chicken vasculature. J. Histochem. Cytochem. 2003; 51:597–604. [PubMed: 12704207]

Jimenez B, et al. Signals leading to apoptosis-dependent inhibition of neovascularization by thrombospondin-1. Nat. Med. 2000; 6:41–48. [PubMed: 10613822]

Kuchibhotla S, et al. Absence of CD36 protects against atherosclerosis in ApoE knock-out mice with no additional protection provided by absence of scavenger receptor A I/II. Cardiovasc. Res. 2008; 78:185–196. [PubMed: 18065445]

Kunz A, et al. Nuclear factor-kappa B activation and postischemic inflammation are suppressed in CD36-null mice after middle cerebral artery occlusion. J. Neurosci. 2008; 28:1649–1658. [PubMed: 18272685]

Loy DN, et al. Temporal progression of angiogenesis and basal lamina deposition after contusive spinal cord injury in the adult rat. J. Comp. Neurol. 2002; 445:308–324. [PubMed: 11920709]

Magnuson DS, et al. Functional consequences of lumbar spinal cord contusion injuries in the adult rat. J. Neurotrauma. 2005; 22:529–543. [PubMed: 15892599]

Mahoney ET, et al. ADAM8 is selectively up-regulated in endothelial cells and is associated with angiogenesis after spinal cord injury in adult mice. J. Comp. Neurol. 2009; 512:243–255. [PubMed: 19003792]

Marciniak SJ, et al. Activation-dependent substrate recruitment by the eukaryotic translation initiation factor 2 kinase PERK. J. Cell Biol. 2006; 172:201–209. [PubMed: 16418533]

Mautes AE, et al. Vascular events after spinal cord injury: contribution to secondary pathogenesis. Phys. Ther. 2000; 80:673–687. [PubMed: 10869130]

Mungrue IN, et al. CHAC1/MGC4504 is a novel proapoptotic component of the unfolded protein response, downstream of the ATF4-ATF3-CHOP cascade. J. Immunol. 2009; 182:466–476. [PubMed: 19109178]

Myers SA, et al. CD47 knockout mice exhibit improved recovery from spinal cord injury. Neurobiol. Dis. 2011; 42:21–34. [PubMed: 21168495]

National Research Council. Guide for the care and use of laboratory animals. The National Academies Press; Washington, DC: 1996.

Oh J, et al. Endoplasmic reticulum stress controls M2 macrophage differentiation and foam cell formation. J. Biol. Chem. 2012; 287:11629–11641. [PubMed: 22356914]

Ohri SS, et al. Attenuating the endoplasmic reticulum stress response improves functional recovery after spinal cord injury. Glia. 2011; 59:1489–1502. [PubMed: 21638341]

Park YM, et al. CD36 modulates migration of mouse and human macrophages in response to oxidized LDL and may contribute to macrophage trapping in the arterial intima. J. Clin. Invest. 2009; 119:136–145. [PubMed: 19065049]

Park L, et al. Scavenger receptor CD36 is essential for the cerebrovascular oxidative stress and neurovascular dysfunction induced by amyloid-beta. Proc. Natl. Acad. Sci. U. S. A. 2011; 108:5063–5068. [PubMed: 21383152]

Popovich PG, Jones TB. Manipulating neuroinflammatory reactions in the injured spinal cord: back to basics. Trends Pharmacol. Sci. 2003; 24:13–17. [PubMed: 12498725]

Popovich PG, Longbrake EE. Can the immune system be harnessed to repair the CNS? Nat. Rev. Neurosci. 2008; 9:481–493. [PubMed: 18490917]

Rahaman SO, et al. A CD36-dependent signaling cascade is necessary for macrophage foam cell formation. Cell Metab. 2006; 4:211–221. [PubMed: 16950138]

Sakurai M, et al. Endoplasmic reticulum stress induced in motor neurons by transient spinal cord ischemia in rabbits. J. Thorac. Cardiovasc. Surg. 2005; 130:640–645. [PubMed: 16153907]

Scheff SW, et al. Experimental modeling of spinal cord injury: characterization of a force-defined injury device. J. Neurotrauma. 2003; 20:179–193. [PubMed: 12675971]

Seimon TA, et al. Atherogenic lipids and lipoproteins trigger CD36-TLR2-dependent apoptosis in macrophages undergoing endoplasmic reticulum stress. Cell Metab. 2010; 12:467–482. [PubMed: 21035758]

Silverstein RL, et al. Mechanisms of cell signaling by the scavenger receptor CD36: implications in atherosclerosis and thrombosis. Trans. Am. Clin. Climatol. Assoc. 2010; 121:206–220. [PubMed: 20697562]

Thurston G, et al. Permeability-related changes revealed at endothelial cell borders in inflamed venules by lectin binding. Am. J. Physiol. 1996; 271:H2547–H2562. [PubMed: 8997316]

Vladykovskaya E, et al. Lipid peroxidation product 4-hyroxy-trans-2-nonenal causes endothelial activation by inducing endoplasmic reticulum stress. J. Biol. Chem. 2012; 287:11398–11409. [PubMed: 22228760]

West JD, Marnett LJ. Alterations in gene expression induced by the lipid peroxidation product, 4-hydroxy-2-nonenal. Chem. Res. Toxicol. 2005; 18:1642–1653. [PubMed: 16300372]

Whetstone WD, et al. Blood–spinal cord barrier after spinal cord injury: relation to revascularization and wound healing. J. Neurosci. Res. 2003; 74:227–239. [PubMed: 14515352]

Witte I, Horke S. Assessment of endoplasmic reticulum stress and the unfolded protein response in endothelial cells. Methods Enzymol. 2011; 489:127–146. [PubMed: 21266228]

Woo MS, et al. Genetic deletion of CD36 enhances injury after acute neonatal stroke. Ann. Neurol. 2012; 72:961–970. [PubMed: 23280844]

Wu S, et al. Ultraviolet light activates NFkappaB through translational inhibition of IkappaBalpha synthesis. J. Biol. Chem. 2004; 279:34898–34902. [PubMed: 15184376]

Yoshida H. ER stress and diseases. FEBS J. 2007; 274:630–658. [PubMed: 17288551]

Zhou P, et al. The scavenger receptor CD36 contributes to the neurotoxicity of bone marrow-derived monocytes through peroxynitrite production. Neurobiol. Dis. 2011; 42:292–299. [PubMed: 21296664]

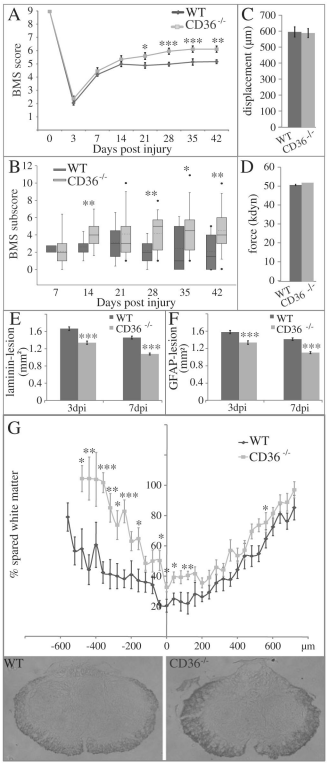

Fig. 1.

CD36 deletion improves functional outcome after moderate spinal cord contusion. (A) Adult CD36$^{-/-}$ mice showed a significant improvement in locomotor recovery by day 21 in (n = 22, ****) relative to wildtype (n = 21, ****), as assessed by the BMS (*p < 0.05, **p < 0.01, ***p < 0.001). Data are means ± SEM. (B) Subscore analysis revealed a similar improvement in hindlimb coordination (*p < 0.05, **p < 0.01). Mean, ****; median, ****; outliers, *****; whiskers, 5th and 95th percentiles. Biophysical assessment of initial injury parameters showed no significant difference between groups with respect to IH impact displacement (C), the best predictor of injury severity (Ghasemlou et al., 2005), or force (D). (E) Deletion of CD36 significantly decreases contusion epicenter lesion area as defined by either (E) laminin or (F) GFAP deposition (WT, n = 4; CD36$^{-/-}$, n = 4 per timepoint; ***p < 0.001). Data are means ± SEM. (G) Deletion of CD36 (n = 16, ****) increases the percentage of spare white matter relative to WT (n = 10, ****) caudal to and at the injury epicenter 7 weeks post-injury (*p < 0.05, **p < 0.01, ***p < 0.001). Negative values on the x-axis represent μm caudal to injury epicenter. Data are means ± SEM. Images (converted to monochrome) are representative epicenters of Eriochrome cyanine-stained coronal sections.

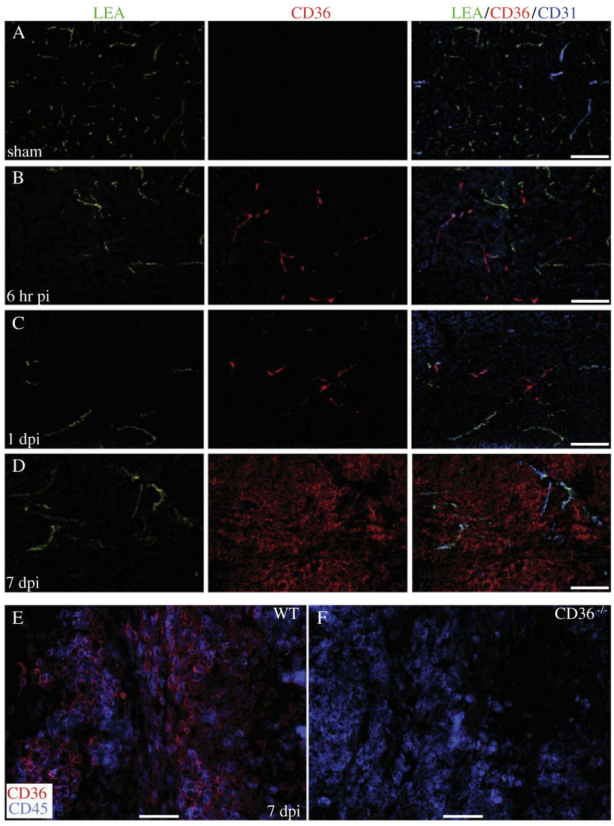

Fig. 2.

CD36 localizes primarily to hypoperfused microvessels and inflammatory cells infiltrating within the contusion epicenter following SCI. CD36 expression (red) is absent in sham uninjured cords (A), but is upregulated in epicenter and penumbral CD31-expressing microvessels (blue) by 6 (B) and 24 (C) hours post-injury, especially within hypoperfused microvessels, as detected by an absence of LEA (green). By 7 dpi (D–E), CD36 expression is significantly reduced in microvessels but highly expressed in invading $CD45^{+}$ inflammatory cells. (F) No expression was detectable in $CD36^{-/-}$ mice. Bars = 100 μm.

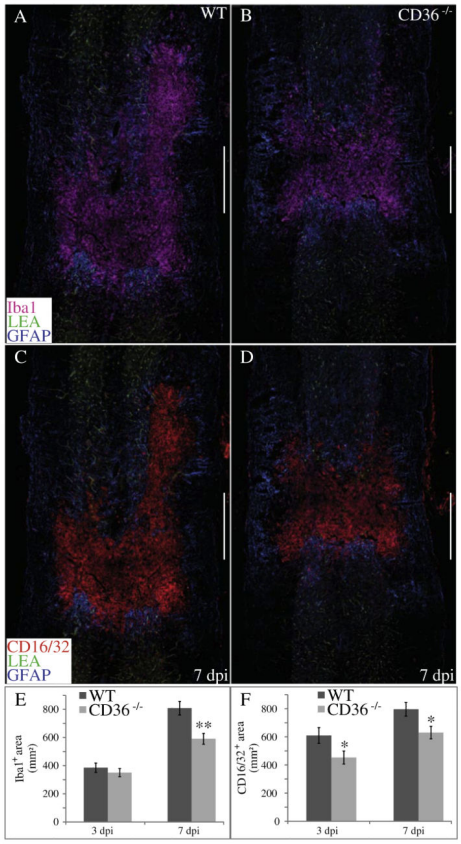

Fig. 3.

CD36$^{-/-}$ mice exhibit a reduced presence of heterodomain macrophages following SCI. The mean area within the injury heterodomain positive for the inflammatory markers Iba1 (pink, A, B, E) and CD16/CD32 (red, B, D, F) were significantly reduced by 7 dpi (**$p < 0.01$, *$p < 0.05$) in CD36$^{-/-}$ mice. GFAP and LEA are shown in blue and green, respectively (A–D). Data are means ± SEM (WT, n = 4; CD36$^{-/-}$, n = 4 per timepoint). Bars = 500 μm.

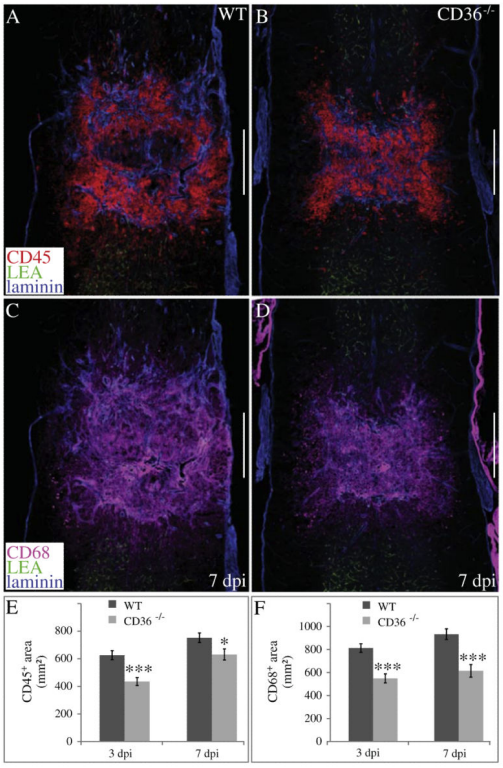

Fig. 4.

Deletion of CD36 reduces localization of CD45 and CD68-positive inflammatory cells within the contusion following SCI. The mean area within the injury heterodomain positive for the hematopoietic markers CD45 (red, E, G) and CD68 (pink, F, H) were significantly reduced by 3 and 7 dpi (***$p < 0.001$, *$p < 0.05$) in $CD36^{-/-}$ mice. Laminin (blue) and LEA (green) are shown (A–D). Data are means ± SEM (WT, n = 4; $CD36^{-/-}$, n = 4 per timepoint). Bars = 500 μm.

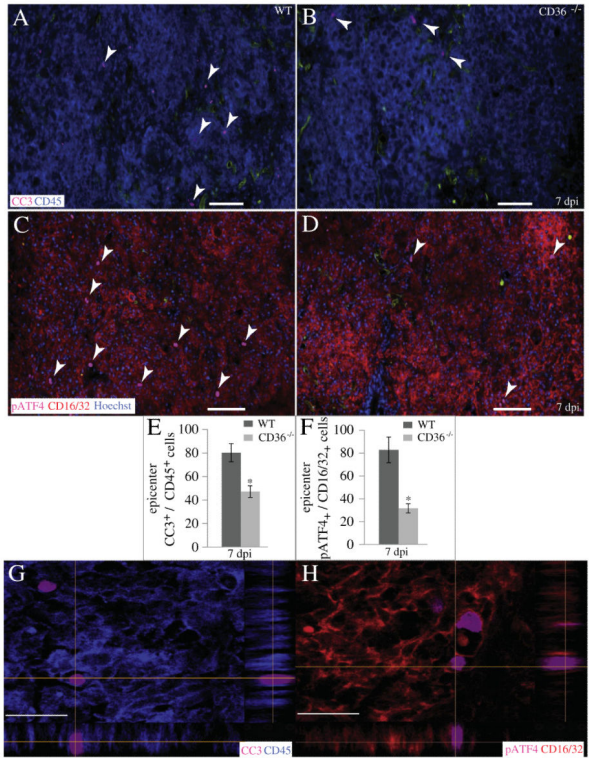

Fig. 5.

Fewer inflammatory cells within the injury epicenter of CD36$^{-/-}$ mice exhibit an ER stress response or apoptosis. (A, B, E, G) Cells positive for both CD45 (blue) and cleaved caspase-3 (CC3, pink) within the injury epicenter were counted 7 days post-contusion. LEA is shown in green. (C, D, F, H) Cells positive for both CD16/CD32 (red) and phospho-ATF4 (pink) within the injury epicenter were counted at 7 dpi. LEA is shown in green and Hoechst in blue. Data are means ± SEM (WT, n = 4; CD36$^{-/-}$, n = 4; *p < 0.05). Bars = 100 μm. (G, H) Confocal imaging demonstrates localization of CC3 or phospho-ATF4 within CD45 or CD16/32-positive cells, respectively. XZ and YZ planes are indicated by the perpendicular orange lines. Bars = 25 μm.

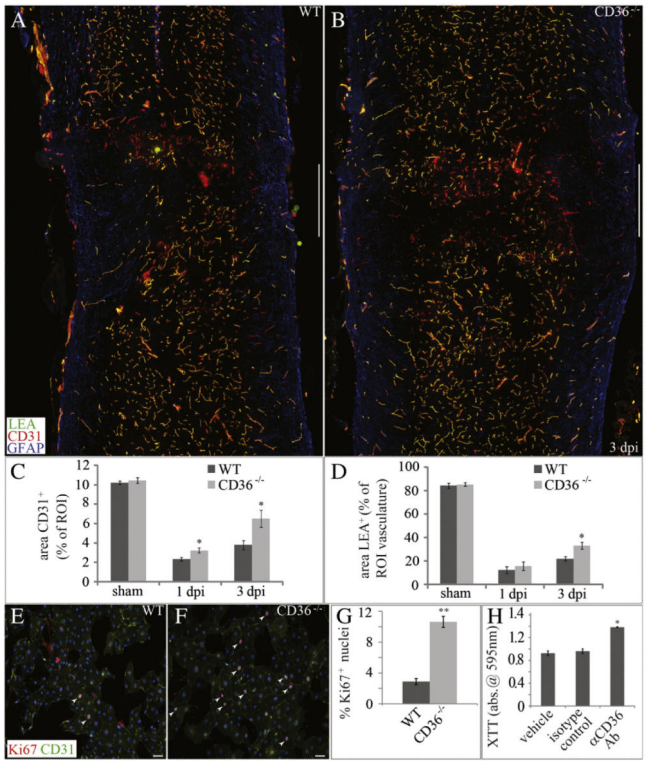

Fig. 6.

Deletion of CD36 improves injury heterodomain vascularity as well as vascular perfusion following SCI. (A–C) The percentage area of $CD31^{+}$ microvessels (red) within the injury heterodomain was significantly higher in $CD36^{-/-}$ mice both 1 and 3 dpi. (A, B, D) The percentage area of LEA (green), a marker for vascular perfusion, within the injury heterodomain was significantly higher in $CD36^{-/-}$ mice 3 dpi. GFAP is shown in blue (A, B). Data are means ± SEM (WT, n = 4; $CD36^{-/-}$, n = 4 per timepoint; *$p < 0.05$). Bars = 500 μm. (E–G) CNS-derived, $CD31^{+}$ (green) endothelial cells from $CD36^{-/-}$ mice exhibit a significantly higher percentage of $Ki67^{+}$ nuclei (red) in vitro. Hoechst is shown in blue. Data are means ± SEM (**$p < 0.01$, n = 4). Bars = 100 μm. (H) Functional blockade of CD36 increases cell proliferation of WT endothelial cells in vitro as assessed by XTT metabolism. Data are means ± SEM (*$p < 0.05$, n = 4).

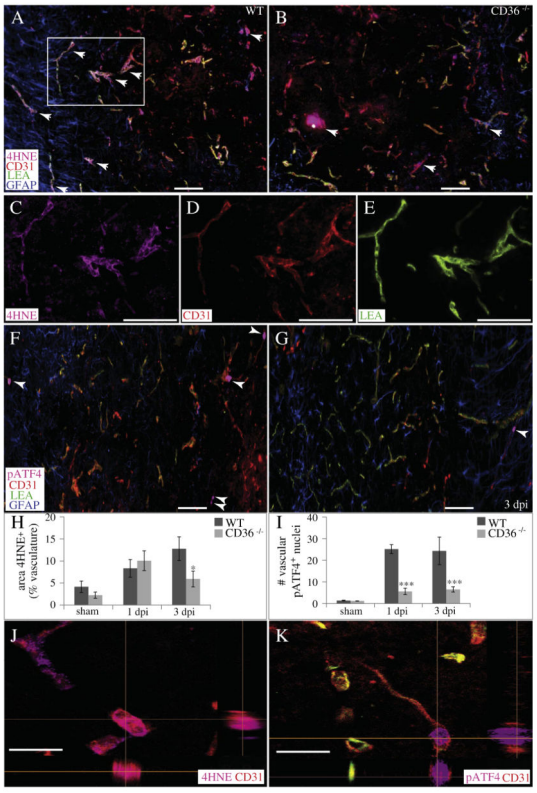

Fig. 7.

CD36 ablation decreases vascular oxidative stress and ER stress responses following SCI. (A–E, H, J) The percentage of injury heterodomain $CD31^{+}$ (red) microvessels which co-localize with the oxidative stress marker 4HNE (pink) is significantly reduced in $CD36^{-/-}$ mice by 3 dpi. (F) The number of injury heterodomain $CD31^{+}$ (red) microvessels which colocalize with the ERSR marker phospho-ATF4 (pink) is significantly reduced in $CD36^{-/-}$ mice (G) at 1 and 3 dpi (I). GFAP (blue) and LEA (green) are also shown. Data are means ± SEM (WT, n = 4; $CD36^{-/-}$, n = 4 per timepoint; *p < 0.05, ***p < 0.001). Bars = 100 μm. Confocal imaging demonstrates co-localization of 4HNE (J) or phospho-ATF4 (K) within the $CD31^{+}$ microvasculature. XZ and YZ planes are indicated by the perpendicular orange lines. Bars = 25 μm.

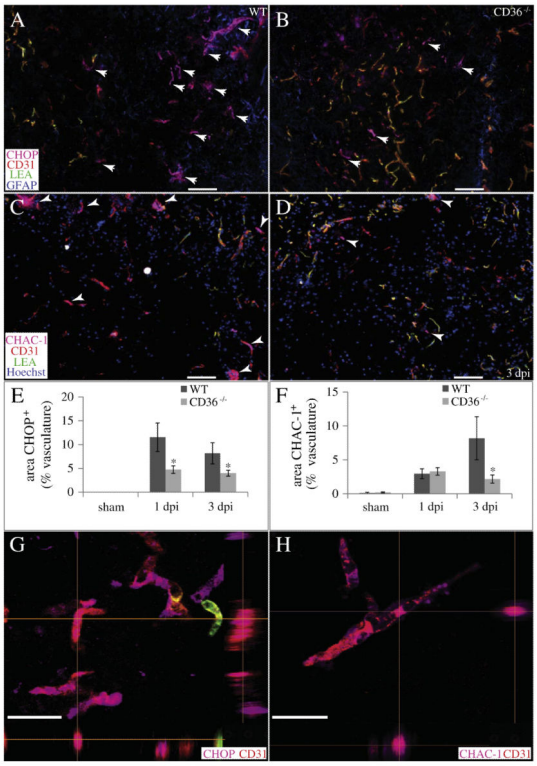

Fig. 8.

CD36 deletion decreases vascular ER stress responses and pro-apoptotic signaling following SCI. (A, B, E, G) The percentage of injury heterodomain $CD31^{+}$ (red) microvessels which co-localize with the pro-apoptotic ERSR protein CHOP (pink) is significantly reduced in $CD36^{-/-}$ mice at 1 and 3 dpi. GFAP (blue) and LEA (green) are also shown. (C, D, F, H) The percentage of injury heterodomain $CD31^{+}$ (red) microvessels which co-localize with pro-apoptotic CHAC-1 (pink) is significantly reduced in $CD36^{-/-}$ mice by 3 dpi. Hoechst (blue) and LEA (green) are also shown. Data are means ± SEM (WT, n = 4; $CD36^{-/-}$, n = 4 per timepoint; *$p < 0.05$). Bars = 100 μm. Confocal imaging reveals co-localization of CHOP (G) or CHAC-1 (H) within the $CD31^{+}$ microvasculature. XZ and YZ planes are indicated by the perpendicular orange lines. Bars = 25 μm.

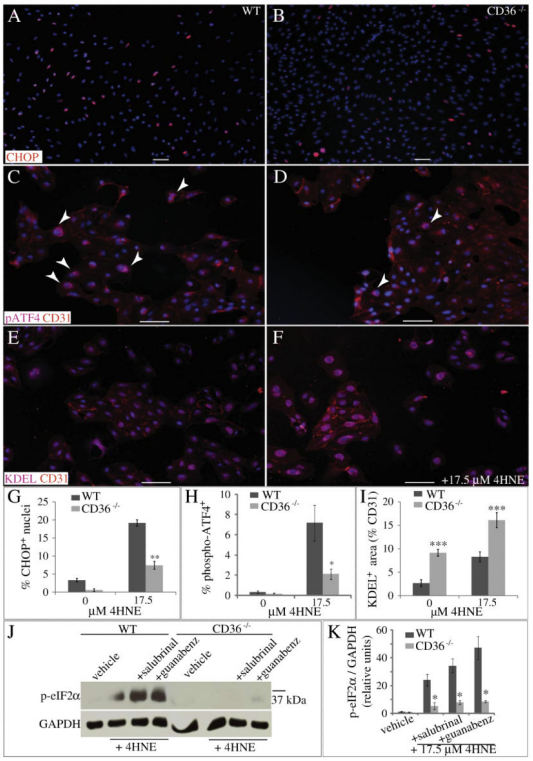

Fig. 9.

Exogenous 4HNE induces diminished ERSR in CD36$^{-/-}$ endothelial cells in vitro. (A, B, G) The percentage of CHOP^{+} (red) nuclei of CD36$^{-/-}$ CNS endothelial cells is significantly reduced after 4HNE administration (**$p < 0.01$, $n = 4$). (C, D, H) The percentage of phospho-ATF4^{+} (pink) endothelial cells derived from CD36$^{-/-}$ mice is significantly reduced after 4HNE administration (*$p < 0.05$, $n = 3$). (E, F, I) The percent area of CD31^{+} (red) endothelial cells co-localized with the ER-localized protein marker KDEL (pink) is significantly increased in CD36$^{-/-}$ endothelial cells both before and after 4HNE (***$p < 0.001$, $n = 4$). Hoechst (blue) is also shown. Data are means ± SEM. Bars = 100 μm. (J–K) Induction of phosphoeIF2α by 17.5 μM 4HNE is significantly reduced in CD36$^{-/-}$ endothelial cells, even in the presence of 100 μM of the phosphatase inhibitors salubrinal or guanabenz. Data are means ± SEM ($n = 3$ each; *$p < 0.05$).

Table 1

Antibodies.

Antigen/clone	Antibody type	Catalog #	Dilution	Vendor
4HNE	prb	393207	1:250	Millipore, Billerica, MA
CD16/CD32/2.4G2	mr	553142	1:150	BD Pharm., San Diego, CA
CD36/CRF-D2712	mm	552544	1:100	BD Pharm., San Diego, CA
CD36/JC63.1	mm	ab23680	10 μg/ml	Abcam, Cambridge, MA
CD45/IBL-5/25	mr	CBL1326	1:150	Millipore, Billerica, MA
CD68/ED1	mm	MAB1435	1:100	Millipore, Billerica, MA
CHAC1	prb	ab76386	1:100	Abcam, Cambridge, MA
CHOP	prb	DDIT3	1:200	Sigma, St. Louis, MO
CHOP/9C8	mm	MA1-250	1:150	Thermo Sci.,Waltham, MA
Cleaved caspase-3	prb	9661	1:250	Cell Signaling, Danvers, MA
GAPDH/6C5	mm	MAB374	1:7500	Millipore, Billerica, MA
GFAP	pc	AB5541	1:500	Millipore, Billerica, MA
Iba1	prb	019-19741	1:200	Wako, Richmond, VA
KDEL/10C3	mm	ab12223	1:150	Abcam, Cambridge, MA
Ki67	prb	VP-K451	1:500	Vector Labs, Burlingame, CA
Laminin	prb	L9393	1:100	Sigma, St. Louis, MO
PECAM/MEC13.3	mr	550274	1:100	BD Pharm., San Diego, CA
Phospho-ATF4	prb	ab28830	1:250	Abcam, Cambridge, MA
Phospho-eIF2α	prb	44729G	1:1000	Invitrogen, Camarillo, CA
PMN/7/4	mr	MCA7716a	1:150	AbD Serotec, Raleigh, NC
vWF	prb	A0082	1:200	Dako, Carpinteria, CA
Mouse IgG isotype control	–	08-6599	–	Invitrogen, Carlsbad, CA
Rabbit IgG isotype control	–	08-6199	–	Invitrogen, Carlsbad, CA
Rat IgG isotype control	–	ab37361	–	Abcam, Cambridge, MA
Chicken IgG isotype control	–	ab37382	–	Abcam, Cambridge, MA
Mouse IgA control/M18-254	–	553476	10 μg/ml	BD Pharm., San Diego, CA

prb = polyclonal rabbit; mr = monoclonal rat; mm = monoclonal mouse; pc = polyclonal chicken.